Efficient Eosin Y Dye-Sensitized Solar Cell Containing Br^-/Br_3^- Electrolyte

Zhong-Sheng Wang,* Kazuhiro Sayama, and Hideki Sugihara*

Solar Light Energy Conversion Group, Energy Electronics Institute, National Institute of Advanced Industrial Science and Technology (AIST), 1-1-1, Higashi, Tsukuba, Ibaraki 305-8565, Japan

Received: June 17, 2005; In Final Form: September 1, 2005

We found that Br^-/Br_3^- is more suitable than an I^-/I_3^- couple in dye-sensitized solar cells in terms of higher open-circuit photovoltage (V_{oc}) production and higher overall energy conversion efficiency (η) if the dye sensitizer has a more positive potential than that of Br^-/Br_3^-. Under simulated AM1.5 one sun, an eosin Y dye-sensitized solar cell containing 0.4 M LiBr + 0.04 M Br_2 electrolyte in acetonitrile yielded a short-circuit photocurrent (J_{sc}) of 4.63 mA cm^{-2}, V_{oc} of 0.813 V, and fill factor (FF) of 0.693, corresponding to 2.61% of η. Under the same conditions except for the electrolyte 0.4 M LiI + 0.04 M I_2 in acetonitrile instead, the device produced 1.67% of η (J_{sc} = 5.15 mA cm^{-2}, V_{oc} = 0.451 V, FF = 0.721). Replacement of I^-/I_3^- with Br^-/Br_3^- in eosin Y dye-sensitized solar cells yielded a significant increase in V_{oc} offset by slight decreases in J_{sc} and FF, leading to an increase in η by 56%. The significant gain in V_{oc} was attributed to the enlarged energy level difference between the redox potential of the electrolyte and the Fermi level of TiO_2 and the suppressed charge recombination as well. The rate for charge recombination between bromine and the injected electrons was determined to be first order in bromine.

Introduction

Dye-sensitized solar cells (DSSCs) are of great scientific and industrial interest due to their high efficiency and low cost.[1] The DSSCs comprise five major components: (1) conductive mechanical support, (2) nanocrystalline semiconductor film, (3) dye sensitizer, (4) redox couple, and (5) Pt counter-electrode, among which the dye-sensitized nanocrystalline semiconductor oxide, which is called photoelectrode, is at the heart of the DSSC. The cell performance is usually evaluated by two tests. One is the action spectrum, incident photon-to-electron conversion efficiency (IPCE) plotted as a function of excitation wavelength (λ). IPCE is defined as

$$\mathrm{IPCE} = \frac{1240 J_{ph}(\lambda)}{\lambda P(\lambda)} \quad (1)$$

where J_{ph} is the photocurrent density (μA cm^{-2}) produced at a certain wavelength (λ (nm)) with power of $P(\lambda)$ (W m^{-2}). The other test is the current−voltage curve, where the energy conversion efficiency (η) can be derived from the short-circuit photocurrent (J_{sc}), open-circuit photovoltage (V_{oc}), fill factor (FF), and the incident light power (P) according to

$$\eta = \frac{J_{sc} V_{oc} \mathrm{FF}}{P} \quad (2)$$

In a DSSC, charge-transfer processes are illustrated in Figure 1.[2] The dye sensitizer absorbs a photon, and the resulting excited-state injects an electron to the conduction band of TiO_2. The resultant oxidized dye is quickly reduced back to its original state by the reduced species (Red) in the electrolyte; this process is usually called dye regeneration. Red is oxidized to its oxidized form (Ox), and the latter is subsequently reduced back to the Red through accepting electrons at the platinum counter-electrode. Efficient operation of DSSCs relies on both efficient electron injection and efficient dye regeneration. The lowest unoccupied molecular orbital (LUMO) energy level should be sufficiently higher than the conduction band edge minimum (E_{CB}) for efficient electron injection,[3] and meanwhile the potential of the redox couple in the electrolyte (E_{redox}) should be higher than the highest occupied molecular orbital (HOMO) energy level for efficient dye regeneration,[4] which is key to the sustained photocurrent production. The maximum voltage of a DSSC under illumination corresponds to the difference of the Fermi level (E_f) and the redox potential of the electrolyte.

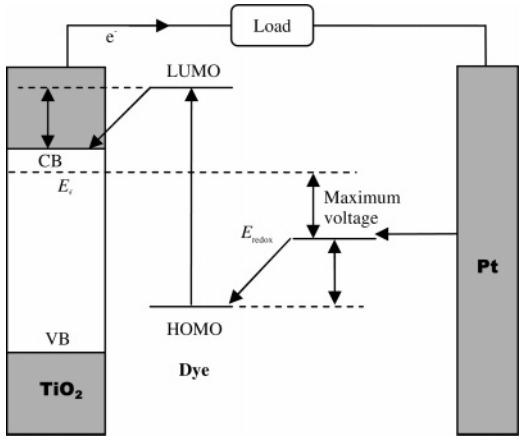

Figure 1. Schematic energy diagram for a dye-sensitized solar cell.

To improve the J_{sc}, a lot of dye sensitizers including ruthenium complexes[5] and metal-free organic dyes,[6] toward broad absorption in the spectral range between 300 and 1000 nm, have been designed and synthesized for their uses in DSSC. The ideal dye sensitizer for the DSSC converting standard AM1.5 sunlight to electricity should absorb all light below a threshold wavelength of about 920 nm, and its HOMO and

* Corresponding author: E-mail: zs.wang@aist.go.jp or wzs64@yahoo.com. Tel: +81-29-861-4643. Fax: +81-29-861-6771.

10.1021/jp053260h CCC: $30.25
Published on Web 11/02/2005

LUMO should match well with the redox potential of the redox mediator in the electrolyte and the conduction band edge minimum of the semiconductor, respectively (Figure 1).[7] The highest η achieved so far in DSSCs is 11% obtained from N719,[8] while the highest η for metal-free organic dyes has been reported to be 8%.[9] Compared to the efforts on dye sensitizers, fewer studies on the redox electrolyte have been reported.[10] Several cobalt(II/III) polypyridyl complexes and the $SeCN^-/(SeCN)_3^-$ based ionic liquid electrolyte have been proved to rival the I^-/I_3^- couple in terms of device efficiency.[10] Although V_{oc} can be increased significantly by adding basic additives such as 4-*tert*-butylpyridine into the electrolyte, J_{sc} is decreased to some degree.[11] In addition, surface coating with insulating oxide layer on the TiO_2 surface is effective to increase V_{oc} due to the formation of an energy barrier or negative shift of the flat band.[12] Another possible method to increase V_{oc} is to enlarge the difference $E_{redox} - E_f$. Oskam et al.[13] studied the influence of pseudohalogens, which have higher potentials than that of I^-/I_3^-, on the V_{oc} of the DSSC, but lower V_{oc} than expected was obtained for these electrolytes, suggesting the complexity of photovoltage production compared to the photocurrent generation. Therefore, the challenge to search for new redox couples that are well matched to the sensitizer, while maintaining the advantages of the I^-/I_3^- couple, still remains.

Most DSSCs studied so far employ I^-/I_3^- couple as electrolyte because of its good stability and reversibility. However, the potential of I^-/I_3^- is not well matched with the potentials of currently employed dye sensitizers, thus resulting in V_{oc} loss. For example, the photovoltage loss arising from the potential mismatch is ~0.4 V for the N719 dye.[4] In particular, some dyes such as eosin Y, which have more positive potentials than $E(Br^-/Br_3^-)$, may yield much larger V_{oc} loss in the case of the I^-/I_3^- couple present in the electrolyte. However, if the Br^-/Br_3^- couple is used in place of the I^-/I_3^- couple for DSSCs containing these dyes, V_{oc} enhancement is expected. In this paper, eosin Y dye-sensitized solar cells with Br^-/Br_3^- as redox electrolyte are presented, along with discussion of charge recombination mechanism between conduction band electrons and bromine. It was found that dyes with more positive potential than $E(Br^-/Br_3^-)$ were able to produce higher V_{oc} and η using Br^-/Br_3^- couple as electrolyte than those using I^-/I_3^- couple as electrolyte.

Experimental Section

Reagents. Eosin Y (acid form) and coumarin 343 were purchased from Aldrich. NKX-2677 was available from our previous study.[14] N719 was obtained from Solaronix SA. Acetonitrile, LiBr, Br_2, LiI, and I_2 were obtained from Wako Pure Chemical Industries Ltd. and used as received. The redox electrolytes used in this study were prepared in a drybox by dissolving weighed amounts of reagents in acetonitrile.

Fabrication of the Dye-Sensitized TiO_2 Solar Cells. TiO_2 paste made from 23 nm nanoparticles, ethyl cellulose, and α-terpineol was prepared using a published method.[15] Transparent TiO_2 films (6 μm), monitored with a Tenchor Alpha-Step 500 surface profiler, were fabricated by screen printing the TiO_2 paste on the conductive glass (TCO, F-doped SnO_2, 10 Ω/□, Nippon Sheet Glass Co., Japan) followed by calcinations at 525 °C for 2 h with a rising rate of 10 °C/min. The film size was 0.5 cm × 0.5 cm. The $TiCl_4$-pretreated film[16] was soaked in the dye solution (0.3 mM in acetonitrile/tertbutanol, volume ratio of 1/1) for at least 12 h. The dye-loaded TiO_2 as working electrode and the platinized TCO glass as counter-electrode were assembled into a sealed device using a hot-melt Surlyn (30 μm thick). The redox electrolyte was introduced into the interspace between the working and the counter-electrodes through two predrilled holes on the back of the counter-electrode. The two holes were sealed up using a Surlyn film, on which a thin glass slide was pressed under heat.[17]

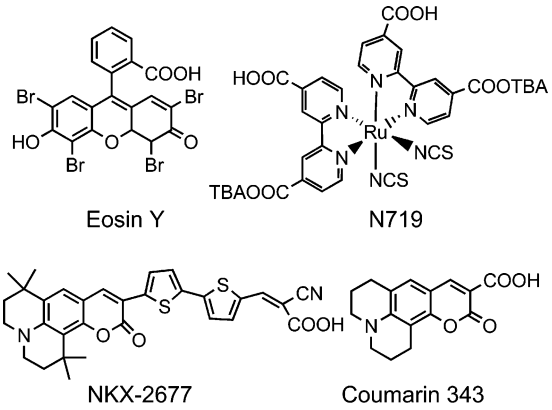

Figure 2. Molecular structure of the dyes studied.

Photovoltaic Measurement. The simulated AM1.5 solar light came from a solar simulator (Wacom Co., Japan, WXS-80C-3 with a 300-W Xe lamp and an AM 1.5 filter). *I*−*V* curves were measured with a dc voltage current source/monitor (Advantest, R6243), which was controlled by a computer. The incident light intensity was calibrated with a standard Si solar cell equipped with a KG-5 filter, which was produced by Japan Quality Assurance Organization. IPCE action spectra were recorded on a CEP-99W system (Bunkoh-Keiki Co. Ltd., Japan). The intensity of incident monochromatic light was calibrated with a Si photodiode (Bunkoh-Keiki Co. Ltd., Japan).

Analytical Instruments. UV−vis absorption spectra of the dye-loaded film were recorded on a Shimadzu model 3100 UV−vis−NIR spectrophotometer in transmission mode. The conductivity of the electrolytes used in this study was measured with a conductivity meter (CM-60G, Analyticon Instruments Co., USA). A two-electrode electrochemical cell, consisting of a Pt ultramicroelectrode (25.0 μm in diameter) as working electrode and a Pt wire as counter-electrode, was employed to measure the diffusion coefficient with a CH 610B electrochemical analyzer. The electrolyte was degassed with N_2 for 20 min prior to potential scan. Impedance spectra were measured with an impedance/Gain-Phase analyzer (Solartron SI 1260) connected with a potentiostat (Solartron SI 1286) under illumination of AM1.5 simulated solar light (100 mW cm^{-2}) from a solar simulator (Wacom). The spectra were scanned in a frequency range of 10^5−0.1 Hz at room temperature. The applied bias and ac amplitude were set at open-circuit condition and 10 mV, respectively.

Results

Comparison of Solar Cell Performance with Different Redox Couples. Eosin Y,[18] coumarin 343,[19] N719,[20] and NKX-2677,[14] whose structures are shown in Figure 2, have been studied as dye sensitizers in DSSCs using I^-/I_3^- electrolyte. All the four dyes can produce photocurrents efficiently, because they meet the thermodynamic requirements for electron injection and dye regeneration by iodide. When the redox couple I^-/I_3^- is replaced with Br^-/Br_3^-, the driving force for dye regeneration is reduced and meanwhile the difference of $E_{redox}-E_f$ is enlarged, which will influence the V_{oc} and J_{sc} to some extent. Table 1 lists the HOMOs for the four dyes and summarizes the cell performance using 0.4 M LiBr + 0.04 M Br_2 or 0.4 M LiI +

TABLE 1: Solar Cell Performance[a] under Simulated AM1.5 Full Sun for Various Dyes

	electrolyte[b]	J_{sc}/mA cm^{-2}	V_{oc}/V	FF	η	HOMO (V vs NHE)
Coumarin 343	0.4 M LiI + 0.04 M I_2	3.25	0.274	0.604	0.54	1.21[21]
	0.4 M LiBr + 0.04 M Br_2	3.83	0.428	0.426	0.70	
Eosin Y	0.4 M LiI + 0.04 M I_2	5.15	0.451	0.721	1.67	1.15[23]
	0.4 M LiBr + 0.04 M Br_2	4.63	0.813	0.693	2.61	
N719	0.4 M LiI + 0.04 M I_2	15.67	0.554	0.634	5.50	1.09[20]
	0.4 M LiBr + 0.04 M Br_2	3.51	0.556	0.539	1.05	
NKX-2677	0.4 M LiI + 0.04 M I_2	18.65	0.444	0.514	4.26	0.94[14]
	0.4 M LiBr + 0.04 M Br_2	0			0	

[a] 6 μm nanocrystalline TiO_2 films were used for DSSCs. [b] $E(I^-/I_3^-) = 0.53$ V, $E(Br^-/Br_3^-) = 1.09$ V. All potentials mentioned in this study except Figure 5 are against NHE.

0.04 M I_2 in acetonitrile. The HOMO of NKX-2677 is more positive than $E(I^-/I_3^-)$ so that it can produce photocurrent efficiently with I^-/I_3^- couple. However, no photocurrent was generated for NKX-2677 when Br^-/Br_3^- couple was employed because the thermodynamic driving force for dye regeneration was unfavorable due to the less positive HOMO of the dye than $E(Br^-/Br_3^-)$. Using the I^-/I_3^- couple, N719 is proved to be an outstanding dye sensitizer on nanocrystalline TiO_2.[20] It could also produce photocurrents with a Br^-/Br_3^- couple, though the J_{sc} value is much lower than that with an I^-/I_3^- couple. The HOMO of N719 is more positive than $E(I^-/I_3^-)$ but equals $E(Br^-/Br_3^-)$, and therefore much less efficient dye regeneration by bromide than by iodide is expected, which accounts for the lower J_{sc} with the Br^-/Br_3^- couple. The HOMOs for both eosin Y and coumarin 343 are more positive than $E(I^-/I_3^-)$ and $E(Br^-/Br_3^-)$ as well, and therefore comparable photocurrents were observed for both electrolytes. Obviously, only when E_{redox} is sufficiently higher than the HOMO of the dye can the photocurrent be generated efficiently.

Additionally, the FF for every DSSC in Table 1 decreased to some degree upon the redox couple changing from I^-/I_3^- to Br^-/Br_3^-. This is attributed to the decreased conductivity from I^-/I_3^- to Br^-/Br_3^- electrolyte, which will be discussed in the discussion section.

According to Figure 1, the V_{oc} enhancement is expected upon redox couple change. The V_{oc} for eosin Y and coumarin 343 was increased but with different degree. N719 showed similar V_{oc} in both electrolytes. These results in combination with the data from the ref 13 indicate that the mechanism for photovoltage generation is very complicated. For simplicity, we will only discuss the details of eosin Y dye-sensitized solar cells, characterizations of electrolyte, and the charge recombination between injected electrons and bromine in the following sections.

IPCE Action Spectrum. The dashed curve in Figure 3 shows the UV−vis absorption spectrum for eosin Y loaded nanocrystalline TiO_2. A strong absorption peak was observed around 530 nm, with absorption threshold of ~600 nm (2.07 eV). The formal potential (1.15 V vs NHE, all potentials in this text except Figure 5 are reported against NHE) of eosin Y,[21] regarded as HOMO, and the absorption threshold for the dye-loaded TiO_2 film, taken as the 0−0 transition energy (E_{0-0}), yield a LUMO of −0.92 V (LUMO = HOMO − E_{0-0}). Evidently, the higher LUMO (−0.92 V) of the dye than E_{CB} (−0.5 V)[2] of TiO_2 and the lower HOMO (1.15 V) than $E(Br^-/Br_3^-)$ (1.09 V) meet the thermodynamic requirements for both electron injection and dye regeneration (see Figure 1).

Two types of eosin Y dye-sensitized nanocrystalline TiO_2 solar cells employing 0.4 M LiBr + 0.04 M Br_2 in acetonitrile (denoted as device A) or 0.4 M LiI + 0.04 M I_2 in acetonitrile (denoted as device B) are compared in this study. Figure 3 compares the action spectra for devices A and B at the same experimental conditions except the electrolyte constituent. Device B generated a maximum IPCE of 56%, which is comparable to the values for eosin Y sensitization of ZnO (47%)[22] or of TiO_2 (51%)[18] reported previously, while device A produced a maximum IPCE of 47%, a little lower than that for device B. Assuming the electron injection is independent of the redox couple,[13] the lower maximum IPCE for device A than that for device B may be due to the less efficient dye regeneration by Br^- than by I^-. The driving force for dye regeneration by Br^- (HOMO − $E(Br^-/Br_3^-) = 0.06$ V) is much smaller than that by I^- (HOMO − $E(I^-/I_3^-) = 0.62$ V), and therefore less efficient dye regeneration is expected in the case of device A. If a dye has more positive potential than that of eosin Y, dye regeneration may be efficient enough not influencing the maximum IPCE. For example, no noticeable difference in maximum IPCE for coumarin 343 (HOMO = 1.21 V)[23] was observed when redox electrolyte was changed from I^-/I_3^- to Br^-/Br_3^-.

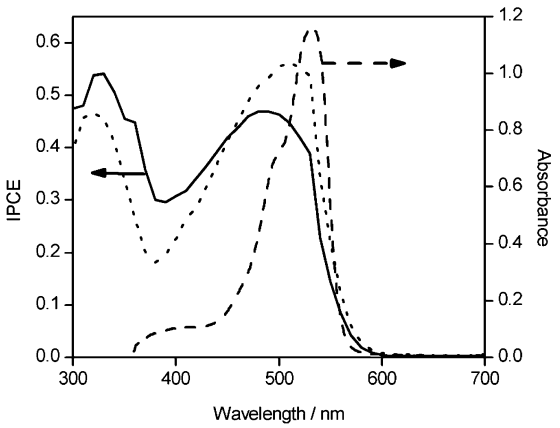

Figure 3. UV−vis absorption spectrum (- - -) of eosin Y loaded 6 μm TiO_2 film with bare TiO_2 as a reference. IPCE action spectra for eosin Y dye-sensitized 6 μm nanocrystalline TiO_2 solar cells with 0.4 M LiBr + 0.04 M Br_2 in acetonitrile (—), and 0.4 M LiI + 0.04 M I_2 in acetonitrile (• • •) as electrolytes, respectively.

One can see from Figure 3 that device A produced larger IPCE values below 450 nm compared to device B. This phenomenon is attributive to the lower absorption of bromine than that of iodine in this spectral region. The electrolyte consisting of Br^-/Br_3^- is superior to that consisting of I^-/I_3^- in terms of lower filtration of light below 450 nm. For this reason, coumarin produced a larger J_{sc} with a Br^-/Br_3^- couple than that with an I^-/I_3^- couple (Table 1). However, the higher IPCEs below 450 nm for eosin Y based device A cannot compensate for the reduced IPCEs above 450 nm compared to device B, resulting in a drop in J_{sc} (see Table 1).

Current−Voltage Characteristics. Figure 4 shows the current−voltage characteristics for device A and device B under

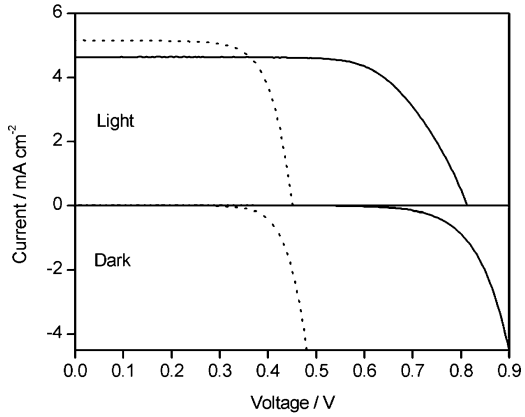

Figure 4. Current−voltage characteristics of eosin Y dye-sensitized 6 μm nanocrystalline solar cells under illumination of 100 mW cm^{-2} simulated AM1.5 solar light (upper) or in the dark (lower) using 0.4 M LiBr + 0.04 M Br_2 in acetonitrile (device A, solid line) or 0.4 M LiI + 0.04 M I_2 in acetonitrile (device B, dotted line) as electrolytes, respectively.

simulated AM1.5 solar light (100 mW cm^{-2}) and in the dark, respectively. At the same experimental conditions, device B produced η of 1.67% (J_{sc} = 5.15 mA cm^{-2}, V_{oc} = 0.451 V, FF = 0.721), while device A generated higher η of 2.61% (J_{sc} = 4.63 mA cm^{-2}, V_{oc} = 0.813 V, FF = 0.693). The η was increased by 56% from device B using I^-/I_3^- electrolyte over device A using Br^-/Br_3^- electrolyte.

As expected, device A produced a much larger V_{oc} than device B. On one hand, the increased energy level difference between the Fermi level and the formal potential of the redox couple plays a crucial role in V_{oc} generation (see Figure 1). On the other hand, V_{oc} also depends on the dark current that is related to the charge recombination between conduction band electrons and the oxidized half in the electrolyte.[24]

$$Ox + e^- \rightarrow Red \qquad (3)$$

The dark current onset potential is related to the V_{oc}, the larger the dark current onset potential, the larger the V_{oc}. We can see from the dark current−potential plots in Figure 4 that the dark current onset potential is shifted to a larger value from device B to device A, accounting for the V_{oc} enhancement due to electrolyte replacement. Furthermore, the dark current onset shift (0.33 V) is in agreement with the V_{oc} increase (0.36 V).

It should be noted that Br_2 is a strong electrophile and tends to undergo bromination reaction with unsaturated bonds especially in the presence of catalysis or light irradiation, and because of this, the device efficiency and long-term stability will be limited. Considering that eosin Y is a bromine derivative of fluorescin, it is relatively stable in the current experimental conditions. However, to achieve long-term stable DSSCs, the knowledge of dye stability in the presence of Br^-/Br_3^- redox couple under light illumination is highly needed.

Discussion

Electrolyte Conductivity. The conductivity of the electrolyte may affect the FF of DSSCs. Table 2 lists the measured conductivity at 21 °C for various electrolytes containing LiBr and Br_2, together with the performance of DSSCs containing the corresponding electrolyte. At constant concentration of LiBr (0.4 M), as the bromine content increased, both the conductivity and the FF of DSSCs increased. There is evidently a positive correlation between them. The conductivity of I^-/I_3^- electrolytes and the performance of the corresponding DSSCs were also measured, results are listed in Table 3. The conductivity did not increase so significantly as observed in the case of the bromine system. As a consequence, the FF in the DSSCs containing an I^-/I_3^- couple did not change noticeably. In Figure 4, device A showed a lower FF than device B. This can be understood by the fact that 0.4 M LiBr + 0.04 M Br_2 has a lower conductivity (1.04 S m^{-1}) than 0.4 M LiI + 0.04 M I_2 (2.52 S m^{-1}) under the same conditions.

TABLE 2: Conductivity of Electrolytes Containing 0.4 M LiBr and Various Contents of Bromine and the Performance of Corresponding DSSCs. Temperature Was 21 °C

$c(Br_2)$/M	conductivity/S m^{-1}	J_{sc}/mA cm^{-2}	V_{oc}/V	FF	η (%)
0.02	0.86	2.72	0.823	0.657	1.5
0.04	1.04	3.95	0.797	0.691	2.2
0.08	1.25	2.72	0.779	0.722	1.5
0.16	1.68	1.96	0.758	0.737	1.1
0.32	2.46	1.62	0.733	0.753	0.9

TABLE 3: Conductivity of Electrolytes Containing 0.4 M LiI and Various Contents of Iodine and the Performance of Corresponding DSSCs at 21 °C

$c(I_2)$/M	conductivity/S m^{-1}	J_{sc}/mA cm^{-2}	V_{oc}/V	FF	η (%)
0.02	2.49	5.15	0.451	0.721	1.7
0.04	2.52	5.28	0.454	0.720	1.7
0.08	2.54	4.77	0.452	0.740	1.6
0.16	2.62	4.05	0.445	0.715	1.3
0.32	2.87	3.62	0.441	0.726	1.2

The conductivity of electrolyte solution depends on the number of ions present, the mobility of ions, and the temperature. In general, increasing electrolyte concentration leads to increased number of ions present and, hence, increases the conductivity. It is of note, however, that the total concentration for the two electrolyte solutions did not change with addition of Br_2 (or I_2) to the LiBr (or LiI) solution, as a result of the formation of trihalide (see next section). One plausible explanation for the increased conductivity with addition of Br_2 (or I_2) to the LiBr (or LiI) acetonitrile solution is given below. It is reported that the solubility and degree of ionization of trihalide are larger than those of halide in acetonitrile.[25] As a consequence, with increase of the bromine (or iodine) content up to 0.32 M, the number of ions present increases, and thus the conductivity rises. LiI is a stronger electrolyte than LiBr in acetonitrile, and therefore the growth rate of conductivity for I^-/I_3^- with addition of iodine to LiI solution is less significant than that for the Br^-/Br_3^- system with addition of bromine to LiBr solution.

Interfacial Electron Transfer. The back transfer of injected electrons to the oxidized dye sensitizer diminishes the photocurrent generation. To reduce or avoid this current loss, transportation kinetics of Br^- and Br_3^- from and to the counter-electrode should be fast enough to regenerate the dye. The diffusion coefficients for the electroactive species in the electrolyte were measured using a linear sweep voltammogram. Figure 5 shows the current−potential plot for the Br^-/Br_3^- electrolyte at a scan rate of 10 mV s^{-1}. Steady-state anodic and cathodic currents were observed. While two anodic waves were observed, only one cathodic wave was detected, consistent with the previous report.[26] The corresponding reduction and oxidation half reactions are indicated in Figure 5. Since the stability constant related to the reaction $Br^- + Br_2 \rightarrow Br_3^-$ is large ($k_f = 10^7$),[27] it is reasonable to consider a complete conversion from Br_2 to Br_3^- with the excess of Br^-. The concentrations of Br^- and Br_3^- were thus calculated to be 0.36 and 0.04 M, respectively. While the cathodic wave is assigned to the reduction from Br_3^- to Br^-, the two anodic waves reflect the

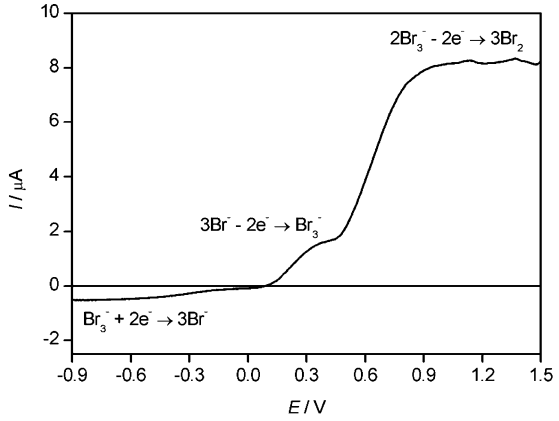

Figure 5. Linear sweep voltammogram of a Pt ultramicroelectrode in 0.4 M LiBr + 0.04 M Br_2 in acetonitrile. Scan rate was 10 mV s^{-1}.

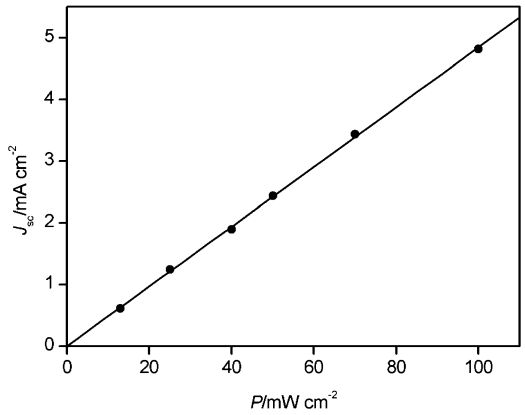

Figure 6. Dependence of J_{sc} on the light intensity (P).

oxidation of Br^- to Br_3^- and the subsequent oxidation of Br_3^- to Br_2, as indicated in Figure 5. The apparent diffusion coefficients (D_{app}) for Br^- and Br_3^- were calculated to be 1.31 $\times$ 10^{-5} and 1.52 $\times$ 10^{-5} cm^2 s^{-1} from anodic (oxidation of Br^-) and cathodic (reduction of Br_3^-) steady-state currents (I_{ss}) according to the following equation

$$I_{ss} = 4ncaFD_{app} \quad (4)$$

where n is the electron transfer number per molecule, F is the Faraday constant, and c is the bulk concentration of the electroactive species.[28] At the same conditions, apparent diffusion coefficients for I^- and I_3^- in 0.4 M LiI + 0.04 M I_2 were determined to be 1.50 $\times$ 10^{-5} and 1.65 $\times$ 10^{-5} cm^2 s^{-1}, respectively, which are similar to those for Br^- and Br_3^-.

To understand the influence of electrolyte diffusion on the cell performance, the dependence of J_{sc} on the light intensity was investigated. Figure 6 depicts a linear dependence of J_{sc} on the light intensity up to one sun. This means that the photocurrent generation is not limited by the diffusion of electrolytes under these experimental conditions. On the basis of these results, we speculate that the decreased maximum IPCE and thus J_{sc} from device B to device A observed in Figures 3 and 4 is ascribed to the insufficient driving force for dye regeneration rather than the transport kinetics of the electrolyte.

Besides the loss channel of photocurrent due to back transfer of injected electron to the oxidized dye, which is intercepted by bromide, another loss mechanism of energy conversion efficiency comes from the charge recombination due to reaction 3.[24] Here, we qualitatively compare the charge recombination in device A and device B. The significant shift of dark current onset potential to a larger value (Figure 4) in combination with the reduced dark current at the same applied potential from device B to device A indicates that the charge recombination was suppressed significantly, partly responsible for the V_{oc} enhancement.

Another piece of evidence supporting the suppression of charge recombination comes from the impedance spectroscopy. Figure 7 shows the impedance spectra for device A and device B at open circuit under AM1.5 one sun. The smaller semicircle and the larger semicircle in the Nyquist plots are attributed to the charge-transfer processes occurring at Pt/electrolyte and TiO_2/dye/electrolyte interface, respectively,[29] which respectively correspond to the high-frequency and mid-frequency peaks in the Bode phase plots. The small semicircle represents the electron transfer from Pt counter-electrode to the oxidized species in the electrolyte, that is, the reduction of the oxidized species to the reduced species, while the large semicircle corresponds to the charge recombination arising from reaction 3.[30] The value of the real part for the cell impedance at the frequency, where the minimum value of the imaginary observed in the larger semicircle of Nyquist plots, is roughly regarded as the charge-transfer resistance at the TiO_2/dye/electrolyte interface mainly due to reaction 3.[31] Evidently, the charge transfer resistance at this interface was increased remarkably from device B to device A according to Figure 7a. Since a slower charge recombination rate corresponds to a larger resistance,[24] this result means in evidence that the charge recombination stemming from reaction 3 was inhibited upon replacing I^-/I_3^- with Br^-/Br_3^-.[32]

In addition, the electron recombination lifetime (τ) can be extracted from the angular frequency (ω_{min}) at the mid-frequency peak in the Bode phase plot using $\tau = 1/\omega_{min}$.[29a] The lifetime

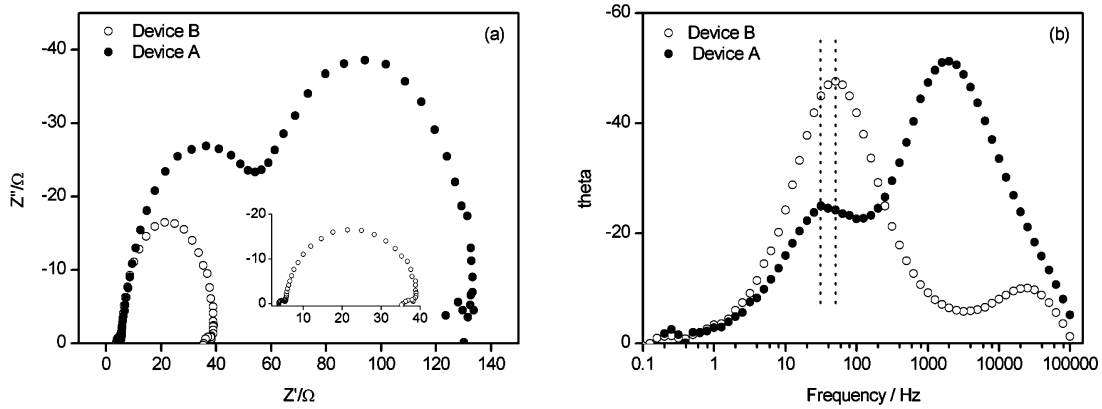

Figure 7. Electrochemical impedance spectra, scanned from 10^5 to 0.1 Hz, for device A and device B, respectively: (a) Nyquist plots; (b) Bode phase plots. The inset in (a) is the magnified Nyquist plot of device B. The applied potential and ac amplitude were set at open-circuit condition and 10 mV, respectively. The cells were measured under illumination of 100 mW cm^{-2} simulated AM1.5 solar light.

is derived to be 32 and 20 ms for Br^-/Br_3^- and I^-/I_3^- redox couple, respectively. The slight increase in electron recombination lifetime also supports that the charge recombination arising from reaction 3 is suppressed upon replacement of I^-/I_3^- with Br^-/Br_3^- couple.

The high-frequency peak in the Bode phase plots also shifted to lower frequency when I^-/I_3^- was replaced with Br^-/Br_3^- couple. Correspondingly in the Nyquist plots, the small semicircle showed a larger resistance for Br^-/Br_3^- couple than that for I^-/I_3^- couple. This means that the reduction of bromine is slower than that of iodine at the Pt counter-electrode. This observation may account for the lower FF in device A than in device B.

Charge Recombination Mechanism. According to the Nernst equation, the redox potential of the Br^-/Br_3^- couple rises positively as the concentration of bromine increases. Therefore, the V_{oc} is expected to increase with increasing the bromine content according to Figure 1. However, contrasting to this expectation, decrease in V_{oc} was observed, as seen in Table 2, which can be interpreted with charge recombination using the following equation

$$V_{oc} = \frac{kT}{qu\alpha} \ln\left(\frac{AI_0}{{n_0}^{u\alpha} k_{et} {c_{ox}}^m}\right) \quad (5)$$

where k is the Boltzmann constant, T is the temperature, q is the electronic charge, n_0 is the electron population in TiO_2 under dark, m and u are the reaction orders of the oxidized species and the electron, respectively, α is the electron-transfer coefficient, c_{ox} is the concentration of the oxidized species in the electrolyte, k_{et} is the rate constant for reaction 3, and A is the ratio of absorbed photon flux to the incident photon flux (I_0).[33] From eq 5, the reaction order of bromine with the conduction band electrons can be determined by

$$-m = \frac{dV_{oc}}{d \ln c_{ox}} \left(\frac{dV_{oc}}{d \ln I_0}\right)^{-1} \quad (6)$$

According to eq 5, V_{oc} should be proportional to the logarithm of light intensity[34] but inversely proportional to the logarithm of bromine concentration. Figure 8 exactly reflects these trends. From the ratio of slopes for the V_{oc} vs log $c(Br_2)$ and V_{oc} vs log P plots,[34] eq 6 yields a value of $m = 1.03$, indicating first order in bromine for the charge recombination between conduction band electrons and bromine. On the basis of the reaction order we derived and the previous electrochemical study[35] on the kinetics of the bromine/tribromide/bromide redox processes, we believe that the charge recombination between the conduction band electrons and the bromine is a kinetically complex reaction involving first dissociation of Br_3^- into Br_2 and Br^- (reaction 7) and then two consecutive reduction steps (reactions 8 and 9), which are comparably rate-limiting.

$$Br_3^- \rightarrow Br^- + Br_2 \quad (7)$$

$$Br_2 + e^- \rightarrow Br^- + Br \quad (8)$$

$$Br + e^- \rightarrow Br^- \quad (9)$$

The charge recombination mechanism between conduction band electrons and bromine is different from that in the case of I^-/I_3^-, where second-order reaction of iodine with conduction band electrons was observed.[33]

Conclusions

Br^-/Br_3^- redox couple was employed in DSSCs and promising results were obtained in this study. The V_{oc} was increased by ~0.36 V for the eosin Y based DSSC when the redox couple was changed from I^-/I_3^- to Br^-/Br_3^-, while the J_{sc} and FF were decreased slightly. We observed that other dyes, such as mordant blue and 5(6)-carboxyfluorescein with higher HOMO than $E(Br^-/Br_3^-)$, could also produce higher V_{oc} and η, while maintaining the J_{sc}. These findings suggest that Br^-/Br_3^- couple may be an alternative to the I^-/I_3^- couple for those dyes with more positive potentials than $E(Br^-/Br_3^-)$ in DSSCs in terms of a good match between the HOMO of the dye and the potential of the redox couple. The increased V_{oc} is explained by the enlarged difference $E_{redox} - E_f$ and the suppressed charge recombination between injected electrons and the oxidized species upon redox couple replacement. While the decreased FF is correlated with the decreased conductivity of the electrolyte, the decreased J_{sc} from device B to device A is ascribed to the insufficient driving force for dye regeneration. To the best of our knowledge, this is the first report that DSSCs using electrolytes other than an I^-/I_3^- couple can yield both higher V_{oc} and higher η compared to the cells with an I^-/I_3^- couple. The efficiency improvement will be further expected after optimization of the electrolyte and if the dye can be engineered to have an extended absorption while maintaining similar IPCE as in the case of the I^-/I_3^- system.

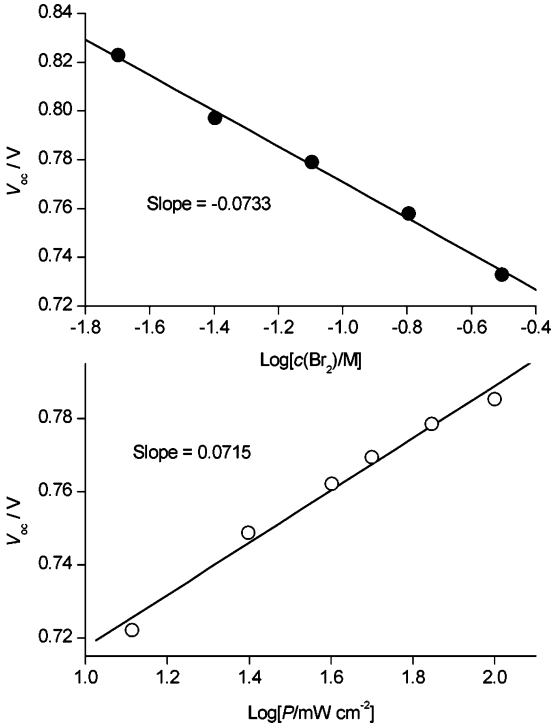

Figure 8. Logarithmic dependence of V_{oc} on the concentration of bromine, $c(Br_2)$ (upper), and the incident light intensity, P (lower).

Acknowledgment. This work was supported by the New Energy and Industrial Technology Development Organization (NEDO) under the Ministry of Economy Trade and Industry. Z.-S. Wang thanks the support from NSFC (20573054).

References and Notes

(1) O'Regan, B.; Grätzel, M. *Nature* **1991**, *353*, 737.
(2) Hagfeldt, A.; Grätzel, M. *Chem. Rev.* **1995**, *95*, 49.
(3) Katoh, R.; Furube, A.; Yoshihara, T.; Hara, K.; Fujihashi, G.; Takano, S.; Murata, S.; Arakawa, H.; Tachiya, M. *J. Phys. Chem. B* **2004**, *108*, 4818.
(4) Grätzel, M. *Prog. Photovolt. Res. Appl*. **2000**, *8*, 171.
(5) (a) Amadelli, R.; Argazzi, R.; Bignozzi, C. A.; Scandola, F. *J. Am. Chem. Soc.* **1990**, *112*, 7099. (b) Renouard, T.; Fallahpour, R.-A.;

Nazeeruddin, Md. K.; Humphry-Baker, R.; Gorelsky, S. I.; Lever, A. B. P.; Grätzel, M. *Inorg. Chem.* **2002**, *41*, 367. (c) Wang, Z.-S.; Huang, C.-H.; Huang Y.-Y.; Zhang, B.-W.; Xie, P.-H.; Hou, Y.-J.; Ibrahim, K.; Qian, H.-J.; Liu, F.-Q. *Sol. Energy Mater. Sol Cells* **2002**, *71*, 261. (d) Wang, Z.-S.; Huang, C.-H.; Zhang, B.-W.; Hou, Y.-J.; Xie, P.-H.; Qian, H.-J.; Ibrahim, K. *New J. Chem.* **2000**, *24*, 567. (e) Wang, P.; Klein C.; Humphry-Baker, R.; Zakeeruddin, S. M.; Grätzel, M. *J. Am. Chem. Soc.* **2005**, *127*, 808. (f) Hara, K.; Sujihara, H.; Tachibana, Y.; Islam, A.; Yanagida, M.; Sayama, K.; Arakawa, H. *Langmuir* **2001**, *17*, 5992. (g) Wang, Z.-S.; Huang, C.-H.; Li, F.-Y.; Weng, S.-F.; Ibrahim, K.; Liu, F.-Q. *J. Phys. Chem. B* **2001**, *105*, 4230.

(6) (a) Wang, Z.-S.; Li, F.-Y.; Huang, C.-H.; Wang, L.; Wei, M.; Jin, L.-P.; Li, N.-Q. *J. Phys. Chem. B* **2000**, *104*, 9676. (b) Wang, Z.-S.; Li, F.-Y.; Huang, C.-H. *Chem. Commun.* **2000**, 2063. (c) Wang, Z.-S.; Li, F.-Y.; Huang, C.-H. *J. Phys. Chem. B* **2001**, *105*, 9210. (d) Ferrere, S.; Zaban, A.; Gregg, B. A. *J. Phys. Chem. B* **1997**, *101*, 4490. (e) Hara, K.; Sato, T.; Katoh, R.; Furube, A.; Ohga, Y.; Shinpo, A.; Suga, S.; Sayama, K.; Sugihara, H.; Arakawa, H. *J. Phys. Chem. B* **2003**, *107*, 597. (f) Wang, Z.-S.; Huang, Y.-Y.; Huang, C.-H.; Zheng, J.; Cheng, H.-M.; Tian, S. J. *Synth. Met.* **2000**, *114*, 201. (g) Kitamura, T.; Ikeda, M.; Shigaki, K.; Inoue, T.; Anderson, N. A.; Ai, X.; Lian, T.; Yangagida, S. *Chem. Mater.* **2004**, *16*, 1806.

(7) Hagfeldt, A.; Grätzel, M. *Acc. Chem. Res.* **2000**, *33*, 269.

(8) Grätzel, M. *J. Photochem. Photobiol. A* **2004**, *164*, 3.

(9) Horiuchi, T.; Miura, H.; Sumioka, K.; Uchida, S. *J. Am. Chem. Soc.* **2004**, *126*, 12218.

(10) (a) Numsbaumer, H.; Moser, J.-E.; Zakeeruddin, S. M.; Nazeeruddin, M. K.; Grätzel, M. *J. Phys. Chem. B* **2001**, *105*, 10461. (b) Sapp, S. A.; Elliott, C. M.; Contado, C.; Caramori, S.; Bignozzi, C. A. *J. Am. Chem. Soc.* **2002**, *124*, 11215. (c) Wang, P.; Zakeeruddin, S. M.; Moser, J.-E.; Humphry-Baker, R.; Grätzel, M. *J. Am. Chem. Soc.* **2004**, *126*, 7164.

(11) Kusama, H.; Arakawa, H. *J. Photochem. Photobiol. A* **2004**, *164*, 103.

(12) (a) Wang, Z.-S.; Huang, C.-H.; Huang, Y.-Y.; Hou, Y.-J.; Xie, P.-H.; Zhang, B.-W.; Cheng, H.-M. *Chem. Mater.* **2001**, *13*, 678. (b) Tennakone, K.; Kumara, G. R. R. A.; Kottegoda, I. R. M.; Perera, V. P. S. *Chem. Commun.* **1999**, 15. (c) Zaban, A.; Chen, S. G.; Chappel, S. Gregg, B. A. *Chem. Commun.* **2000**, 2231. (d) Palomares, E. Clifford, J. N.; Haque, S. A.; Lutz, T.; Durrant, J. R. *J. Am. Chem. Soc.* **2003**, *125*, 475.

(13) Oskam, G.; Bergeron, B. V.; Meyer, G. J.; Searson, P. C. *J. Phys. Chem. B* **2001**, *105*, 6867.

(14) Hara, K.; Kurashige, M.; Dan-oh, Y.; Kasada, C.; Shinpo, A.; Suga, S.; Sayama, K.; Arakawa, H. *New J. Chem.* **2003**, *27*, 783.

(15) Wang, Z. S.; Kawauchi, H.; Kashima, T.; Arakawa, H. *Coord. Chem. Rev.* **2004**, *248*, 1381.

(16) Nazeeruddin, M. K.; Péchy, P.; Renouard, T.; Zakeeruddin, S. M.; Humphry-Baker, R.; Comte, P.; Liska, P.; Cevey, L.; Costa, E.; Shklover, V.; Spiccia, L.; Deacon, G. B.; Bignozzi, C. A.; Grätzel, M. *J. Am. Chem. Soc.* **2001**, *123*, 1613.

(17) Wang, Z.-S.; Hara, K.; Dan-oh, Y.; Kasada, C.; Shinpo, A.; Suga, S.; Arakawa, H.; Sugihara, H. *J. Phys. Chem. B* **2005**, *109*, 3907.

(18) Sayama, K.; Sugino, M.; Sugihara, H.; Abe, Y.; Arakawa, H. *Chem. Lett.* **1998**, 753.

(19) Enea, O.; Moser, J.; Grätzel, M. *J. Electroanal. Chem.* **1989**, *259*, 59.

(20) Nazeerudin, M. K.; Kay, A.; Rodicio, I.; Humphry-Baker, R.; Müller, E.; Liska, P.; Vlachopoulos, N.; Grätzel, M. *J. Am. Chem. Soc.* **1993**, *115*, 6382.

(21) Ryan, M. A.; Fitzgerald, E. C.; Spitler, M. T. *J. Phys. Chem.* **1989**, *93*, 6150.

(22) Yoshida, T.; Terada, K.; Schlettwein, D.; Oekermann, T.; Sugiura, T.; Minoura, H. *Adv. Mater.* **2000**, *12*, 1214

(23) Murakoshi, K.; Yanagida, S.; Capel, M.; Castner, E. W. Jr. *Interfacial Electron-Transfer Dynamics of Photosensitized Zinc Oxide Nanoclusers*; Moskovits, M., Ed.; American Chemical Society: Washington, DC, 1997.

(24) Gregg, B. A.; Pichot, F.; Ferrere, S.; Fields, C. L. *J. Phys. Chem. B* **2001**, *105*, 1422.

(25) Gutmann, V. *Halogen Chemistry*; Academic Press: 1967; Vol. 1.

(26) Iwasita, T.; Giordano, M. C. *Electrochim. Acta* **1969**, *14*, 1045.

(27) Nelson, J. V.; Iwamoto, R. T. *J. Electroanal. Chem.* **1964**, *7*, 218.

(28) Bard, A. J.; Faulkner, L. R. *Electrochemical Methods*: *Fundamentals and Applications*, 2nd ed.; Wiley: Weinheim, Germany, 2001.

(29) (a) Kern, R.; Sastrawan, R.; Ferber, J.; Stangl, R.; Luther, J. *Electrochim. Acta* **2002**, *47*, 4213. (b) Longo, C.; Nogueira, A. F.; Paoli, M.-A.; Cachet, H. *J. Phys. Chem. B* **2002**, *106*, 5925.

(30) The interfacial charge transfer at the TiO_2/dye/electrolyte interface is complex, with many processes, such as charge recombination between injected electrons and oxidized species in the electrolyte or oxidized dyes, the regeneration of oxidized dye with reduced species in the electrolyte et al., occurring at this interface. At open circuit, the injected electrons are accumulated on the TiO_2 surface and not extracted to the external circuit. The electrons and redox species have high concentrations on the TiO_2 surface, ensuring very fast dye regeneration. For this reason, the electron back transfer to the oxidized dye is usually neglected. It is therefore reasonable that the mid-frequency semicircle in the Nyquist plots or the mid-frequency peak in the Bode phase plots is mainly attributed to the charge recombination between injected electrons and oxidized species in the electrolyte because other processes are very fast. The mid-frequency semicircle is clearly assigned to the recapture of electrons by I_3^- ions in ref 29.

(31) Kubo, W.; Murakoshi, K.; Kitamura, T.; Yoshida, S.; Haruki, M.; Hanabusa, K.; Shirai, H.; Wada, Y.; Yanagida, S. *J. Phys. Chem. B* **2001**, *105*, 12809.

(32) Wang, Z.-S.; Yamaguchi, T.; Sugihara, H.; Arakawa, H. *Langmuir* **2005**, *21*, 4272.

(33) Huang, S. Y.; Schlichthörl, G.; Nozik, A. J.; Grätzel, M.; Frank, A. J. *J. Phys. Chem. B* **1997**, *101*, 2576.

(34) Because light intensity P is proportional to the incident photon flux I_0, eq 6 can be written as $-m = \mathrm{d}V_{oc}/\mathrm{d}\ln c_{ox}(\mathrm{d}V_{oc}/\mathrm{d}\ln P)^{-1}$.

(35) Faita, G.; Fiori, G.; Mussini, T. *Electrochim. Acta* **1968**, *13*, 1765.